DESIGN AND CONSTRUCTION

OF AN

IMPROVED ZEEMAN SLOWER

by

Margaret Lynn Harris
Department of Physics

Date Approved: _____

_____
Dr. John E. Thomas, Advisor

_____
Dr. Joshua Socolar

_____
Dr. Daniel Gauthier

A thesis submitted in partial fulfillment of the requirements
for graduation with distinction in physics
in the Department of Physics at
Trinity College, Duke University

2003

Abstract

This document describes the design and construction of a Zeeman slower, a device which takes thermal ^{6}Li atoms with an average velocity of around 1500 m/s and, over a distance of roughly 30 cm, reduces their velocity to a few tens of meters per second in a continuous manner via laser cooling and the Zeeman effect.

The design in this document represents a significant improvement over previous Zeeman slowers. In particular, it is simpler to build, more compact, and should prove much easier to maintain. Although more tests need to be performed before we can draw final conclusions on the new design's efficacy, the results of extensive computer modeling and preliminary testing described in this document indicate a high probability of success.

Acknowledgements

Working in JETLab this past year has been great fun, and I would like to thank everyone there for their help and support. Three cheers and a shiny gold star in particular to Sunidh Jani for assistance with the early coding, Stacy Hemmer and Joe Kinast for helpful Mathematica hints, and Mike Gehm for miscellaneous acts of kindness and encouragement. Additional thanks go to Robert Timberlake and the Physics Shop for help with the technical aspects of the project, and especially for building a slower so beautiful that it resembled modern art.

And then there's John. My advisor's enthusiasm for physics very nearly violates the laws of thermodynamics. His sense of humor, perpetual encouragement, and matter-of-fact nuttiness has kept me excited about Zeeman slowers all year, particularly this past semester when I had more time to spend in the lab. Collecting JETisms seems to be a tradition around the lab, so here are two of my favorites:

"This won't work, but it might."

"Don't go and die on us yet. You haven't finished your thesis."

If my graduate advisor is as kind, helpful, and all-around fun as John Thomas, I will count myself lucky.

I would also like to thank Dan Gauthier and Josh Socolar, the other members of my committee, who have both served as my academic advisor at some point. In addition, my

first physics professor, Al Lee, convinced me to major in physics; although he left Duke during my freshman year, in some sense, I wouldn't have been able to do this work without him.

Finally, I would like to dedicate this thesis to my late grandfather, Howard Schumann, whose quest for a college degree was thwarted by a single class: physics.

Contents

List of Figures

List of Tables

1 Introduction

1.1 The Big Picture

The universe contains two kinds of matter. Some particles – photons, for example – have symmetric wave functions, and are called bosons. Others, like the electrons, protons, and neutrons that make up atoms, have antisymmetric wave functions; these particles are known as fermions. Depending on their composition, atoms can be either fermions or bosons. In an atom like ^{85}Rb, which has an even number of protons, electrons and neutrons, the antisymmetric (fermionic) nature of these component particles cancel each other out, leaving a total particle that behaves like a boson. For other atoms, like the ^{6}Li we use in our experiments at Duke University, the total number of protons, electrons and neutrons is odd, and the atom behaves like a fermion.

Under "normal" circumstances – in our case, "normal" denotes temperatures much greater than the so-called Fermi temperature T_F – the fermionic or bosonic character of matter is unimportant, and the classical picture is sufficient to describe the system [1]. As ^{6}Li atoms approach T_F, however, their quantum nature becomes more apparent, and we begin to observe characteristically fermionic behavior. Very low temperatures $T << T_F$ can, in effect, act as a kind of quantum microscope, allowing us to observe quantum

mechanical effects which until recently had only existed in theoretical descriptions of nature.

For a classical gas, temperature is a measurement of the average kinetic energy in a sample of atoms, so reducing a sample's temperature means reducing the atoms' velocity, which increases their de Broglie wavelength. In the field of atomic, molecular and optical physics, standard tools for producing slow atoms include magneto-optical traps (MOTs), lasers, and the Zeeman slowers described in the next section.

1.2 The Zeeman Slower

At 400 °C, the average speed of ^{6}Li atoms is around 1500 m/s [2]. A good magneto-optical trap (MOT), by contrast, can only capture atoms with velocities of a few tens of meters per second. So, although it is possible in principle to load a MOT directly from a lithium vapor cell, doing so effectively rejects all but the slowest atoms (the tail of the velocity distribution), and is thus both inefficient and time-consuming. The relatively high melting point of lithium also makes construction of lithium vapor traps impractical.

A more efficient method of trap loading [3] uses laser cooling to slow atoms in the longitudinal direction before they enter the MOT. In laser cooling, photons from a laser beam collide with atoms moving in the opposite direction, get absorbed, and are spontaneously re-emitted. Since the direction of emission is random, repeated collisions will result in a net loss of momentum in the direction of the incoming photons, and thus produce a slowing (cooling) of the atoms (Figure 1.1).

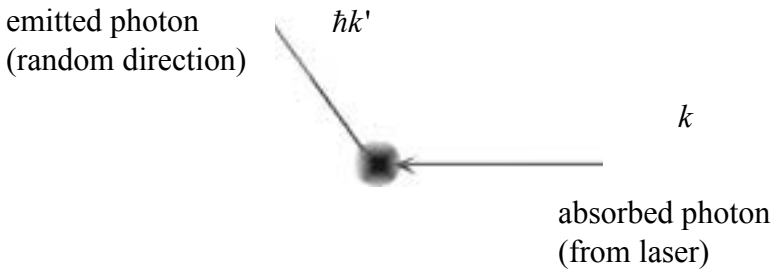

Figure 1.1. Schematic picture of laser cooling.

In order for laser cooling to work, the photons must have a frequency equal to the resonant frequency of the atoms. However, because of the Doppler shift, the photon frequency that the atoms "see" changes as the atoms slow down during the absorption-emission process. Since it is difficult to keep the laser tuned to a constantly changing resonant frequency (as in so-called chirp cooling) [3], and methods that use this approach only produce pulsed sources, one instead uses magnetic fields and the Zeeman effect to tune the atoms – that is, to change their resonant frequency in a way that compensates for the change in speed and keeps them continually on resonance. The system of magnetic coils that produces this result is called a Zeeman slower. Figure 1.2 shows the layout of the slower and the rest of the experimental apparatus.

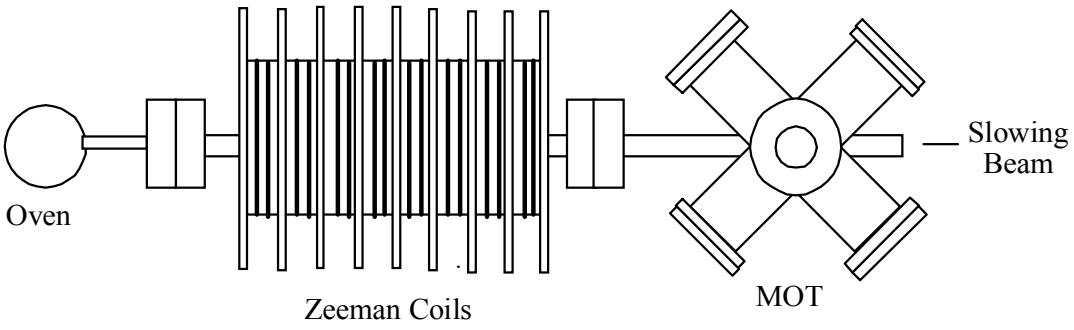

Figure 1.2. Layout of Zeeman slower.

1.3 Rationale for a New Design

Duke's laser cooling and trapping group already has a Zeeman slower, built in 1995 by Thomas Savard, Christopher Baird, and others. At this writing, the original slower is still functioning, and has been an important and effective component of the group's research on cold fermions. However, post-1995 advances in cold-atom theory and long-term observation of our slower's performance in the laboratory led us to believe that the old design is not optimal, and could be improved. In particular, we felt that a shorter, less powerful slower would draw significantly lower currents, take up less space, and prove easier to construct and run, while still producing sufficient quantities of slow atoms for the purpose of our experiment.

Constructing a new slower will also allow the group to perform side experiments and train new members without interrupting progress on the main project. We anticipate the new slower will be the first component of an entirely separate laser-cooling apparatus.

2 Theory

In this section, I provide a brief theoretical explanation of the Zeeman effect. In addition, I describe the scattering process in ^{6}Li and use this to calculate the slower's desired magnetic field taper.

2.1 The Zeeman Effect

As noted in the previous section, the Zeeman effect allows us to keep atoms on resonance with the laser beam despite the presence of the Doppler shift, which changes the beam's frequency in the atoms' reference frame. Although a complete quantum mechanical treatment of the Zeeman effect is outside the scope of this thesis, some explanation is certainly illuminating and relevant to the slow-atoms problem.

In the presence of an external magnetic field $\boldsymbol{B}$, ^{6}Li atoms experience a torque corresponding to a potential energy

$$U = -\boldsymbol{\mu} \cdot \boldsymbol{B} \tag{2.1}$$

where μ is the atom's magnetic dipole moment.

In the quantum mechanical regime, the atom's magnetic dipole moment relates to its orbital angular momentum L by the equation

$$\mu = \frac{eL}{2m_e} \tag{2.2}$$

with e representing the charge of an electron and m_e the electron mass. When the magnetic field is in the z-direction – as for the slower – substituting equation (2.2) into (2.1) gives

$$U = \frac{e}{2m_e} L_z B = m_l \frac{e\hbar}{2m_e} B \tag{2.3}$$

Since angular momentum is quantized, this magnetic field-dependent energy will give rise to a series of equally spaced energy levels shifted from the zero field level by

$$\Delta E = m_l \mu B \, B \tag{2.4}$$

where μ_B is the Bohr magneton, $\mu_B = \frac{e\hbar}{2m_e}$. Physically, these shifted energy levels give rise to a splitting in the atom's spectral lines (Fig. 2.1). This splitting is called the Zeeman effect [4].

Alkali metals such as ^{6}Li belong to a group of materials in which the magnetic field also interacts with the electron spin magnetic moment. This spin interaction gives rise to the so-called *anomalous* Zeeman effect, in which the spectral lines split into doublets, quadruplets, and sextuplets, rather than the pure triplets the semi classical "normal" Zeeman effect predicts.

The general expression for the Zeeman effect ΔE in this case is

$$\Delta E = \frac{e}{2m} \left(\boldsymbol{L} + 2\boldsymbol{S} \right) \cdot \boldsymbol{B} = g_J \mu_B m_i B \qquad (2.5)$$

where g_J, the Lande g factor, is a geometric term arising from the precession of $\boldsymbol{S}$ and $\boldsymbol{L}$ around the total angular momentum $\boldsymbol{J} = \boldsymbol{L} + \boldsymbol{S}$. [5].

The transition we use for ^{6}Li is $| F = 3/2, m_F = 3/2 \rangle \leftrightarrow | F = 5/2, m_F = 5/2)$. The higher energy state is a p orbital with $L_z = 1$ and $S_z = ½$. The lower energy state is an s orbital with $L_z = 0$ and $S_z = ½$. [3]. Since the spin angular momentum does not change as a result of the transition, Eq. 2.5 reduces to

$$\Delta E = \mu_B B \left(L_{z,p} - L_{z,s} \right) = \mu_B B \qquad (2.6)$$

Figure 2.1 shows the relevant transition in ^{6}Li [5].

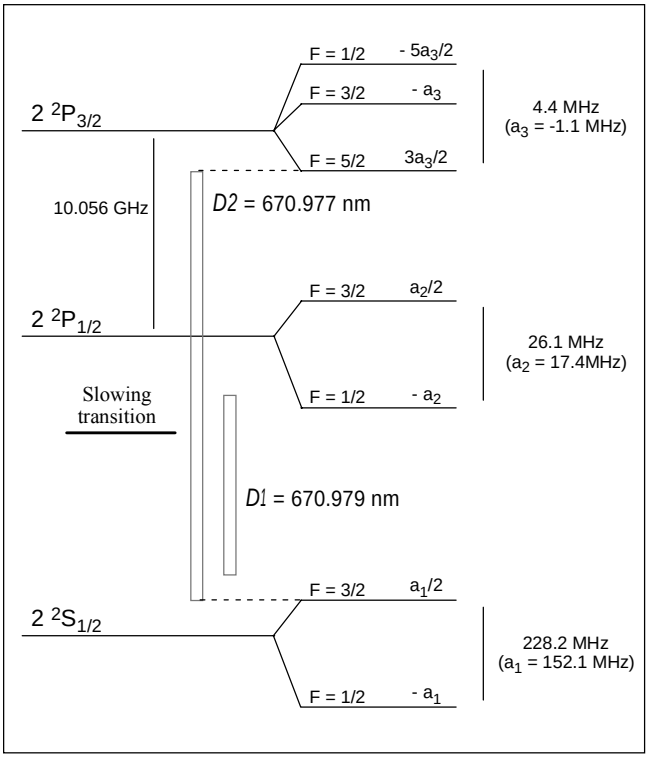

Figure 2.1. Level diagram for ^{6}Li. The slowing transition is labeled D2.

In the next section, we will use this result to calculate the magnetic field the slower must produce to keep atoms on resonance.

2.2 B-field Taper and Scattering Force

To determine the proper shape of the slower's magnetic field, we first examine a parameter Δ, defined as the difference between the laser frequency and the Doppler-shifted, Zeeman-tuned resonant frequency of the ^{6}Li atoms. When the atom is resonant with the laser as it slows down, Δ will be zero.

In the absence of any Doppler shift or external magnetic field,

$$\Delta = \Delta_0 = \omega - \omega_0 \tag{2.7}$$

where ω is the laser frequency and ω_0 is the unshifted atomic resonance frequency. When the Doppler shift and the magnetic field are present,

$$\Delta = \Delta_0 + \frac{v}{\lambda} - \Delta_B \tag{2.8}$$

where v/ λ is the Doppler frequency and Δ_B is the frequency $\frac{\Delta E}{\hbar}$. Using the ΔE we found in calculating the energy level shift due to the Zeeman effect (2.6), setting Δ = 0 and solving for *B (z)*, we find

$$B(z) = \frac{h}{\mu_B}\left(\Delta_0 + \frac{v(z)}{\lambda}\right) \tag{2.9}$$

If we assume constant deceleration, then

$$B(z) = \frac{h}{\mu_B}\left(\Delta_0 + \frac{1}{\lambda}\sqrt{v_i^2 - 2az}\right) \tag{2.10}$$

where v_i is the atom's velocity at $z = 0$ (the front end of the slower) and a is the constant deceleration.

To find a, we first determine the force due to incoming laser photons. In our system, the maximum scattering force an atom experiences due to repeated photon collisions is

$$F_{max} = \frac{\hbar k \Gamma}{2} \tag{2.11}$$

where Γ is the photon scattering rate and k is the photon's wave vector [2]. In ^{6}Li, this force corresponds to a maximum acceleration a_{max} of 1.83 x 10^6 m/s^2, nearly 200,000 times the acceleration of gravity. For most slowers, however, $a = \alpha\, a_{max}$, where $0.5 < \alpha < 0.75$ [2]. Figure 2.2 shows a graph of $B(z)$ with $\alpha = 0.6$, $\Delta_0 = -200$ MHz, $\lambda = 671$ nm, and $v_i = 1100$ m/s.

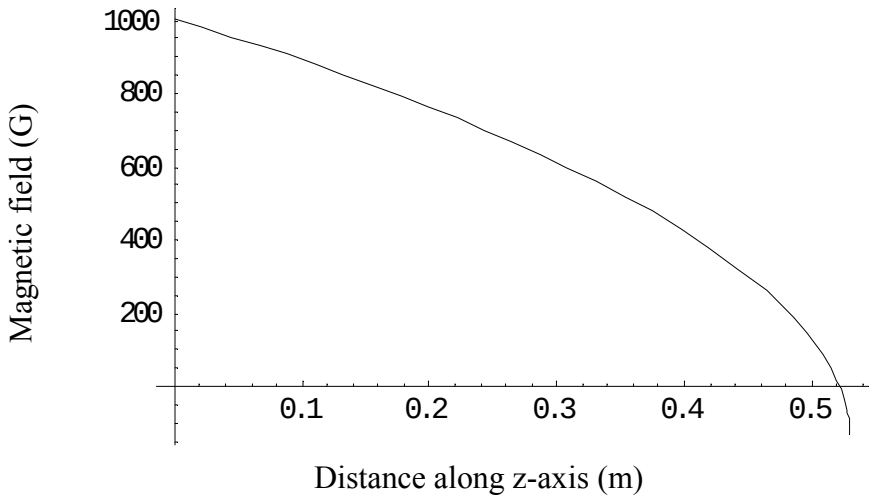

Figure 2.2. Desired magnetic field as a function of z.

3 Design

Designing a Zeeman slower is both a relatively forgiving task and a relatively complicated one. It is forgiving because many different designs will yield a machine capable of producing slow atoms. However, not all designs are created equal, and selecting the optimum solution from among many possibilities requires a number of considerations. In this section, I analyze several design parameters and describe how we arrived at our solution.

3.1 Length

At first glance, the optimum length of the slower might appear to depend entirely on the maximum initial velocity of the atoms we wish to trap, $v_z^{\max}$, and their desired final velocity v_f as they enter the MOT. The relation is familiar from basic kinematics:

$$l = \frac{v_{z_{\max}}^2 - v_f^2}{2a} \tag{3.1}$$

where l is the length of the slower and a is the acceleration given by the force in (2.11). Based on this relation alone, it might seem that a slower several meters in length would be most desirable (assuming sufficient space on the optical table for a slower of that size). A very long slower could, in theory, decelerate nearly all of the thermal atoms down to

trappable velocities, even those which initially occupied the high-velocity "tail" of the Gaussian distribution.

This, however, is not the case. As an atom moves through the slower, the only deceleration it experiences is in the direction opposite the propagating laser beam – in this case, the –z direction. The slowing beam has no effect on the atom's radial velocity v_r, which as a result may be more than an order of magnitude higher than the longitudinal velocity v_f by the time the atom reaches the end of the slower.

Because of this radial velocity, the atom's trajectory through the slower curves outward as it experiences longitudinal deceleration. As the value of v_r increases, the curve grows steeper until at some radial velocity $v_r^{\max}$ the atom's trajectory will take it outside the MOT's trap radius when it reaches the end of the slower. This v_r^{max} and the solid angle it defines (Fig. 3.1) determine the maximum useful length of the slower.

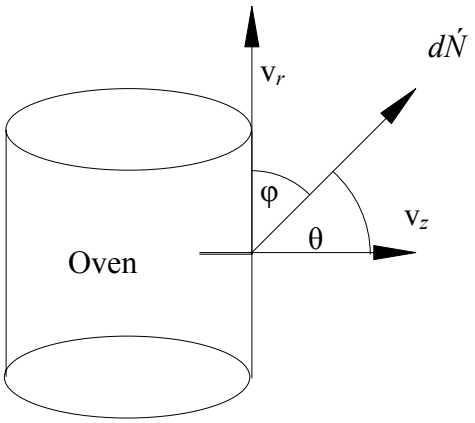

Figure 3.1: Solid angle determined by atoms leaving the oven with v_r and v_z.

Again by simple kinematics, the value of v_r^{max} will be

$$v_r^{\max} = \frac{r_0}{t_b + t_d + t_a} \tag{3.2}$$

where r_0 is the capture radius of the MOT (about 1 cm) and the t_i are the trajectory times (b)efore, (d)uring, and (a)fter deceleration [2]. Each of these trajectory times will depend on the atoms' velocity and the distance the atoms travel at that velocity. Specifically,

$$t_b = \frac{d_b}{v_z^{\max}}$$

$$t_d = \frac{v_z^{\max} - v_f}{a} \tag{3.3}$$

$$t_a = \frac{d_a}{v_f}$$

where d_b is the distance the atoms travel between the oven and the slower and d_a is the distance between the slower and the MOT. In our system, d_b is 10 cm, d_a is about 15 cm, and the desired final velocity v_f is 10 m/s. With thermal velocities in the km/s range, the unslowed atoms will take almost no time to travel from the oven to the slower, so t_b will be negligible even if d_b makes up a large fraction of the slower's total length. However, in the interests of making a conservative estimate of v_r^{max} we will not discard this term. The expression for v_r^{max} is then

$$v_r^{\max} = \frac{r_0}{\left(\frac{d_b}{\sqrt{v_f^2 + 2al}} + \frac{1}{a}\left(\sqrt{v_f^2 + 2al} - v_f\right) + \frac{d_a}{v_f} \right)} \tag{3.4}$$

where the $\sqrt{v_f^2 + 2al}$ terms are simply v_z^{max} obtained by rearranging (2.1).

Now that we have expressions for v_r^{max} and v_z^{max} in terms of l, we can plot the trap loading rate R as a function of the slower length l. We get this rate by calculating the flux

of atoms slowed to the MOT's capture velocity by the Zeeman slower; after performing the necessary solid angle and velocity integrals [2] we find

$$R = \acute{N}\left[1-\exp\left(\frac{-v_{z_{\max}}^2}{\alpha^2}\right)\right]\left[1-\exp\left(\frac{-v_{r_{\max}}^2}{\alpha^2}\right)\right] \tag{3.5}$$

where $\acute{N}$ is the number of atoms leaving the oven per second, $v_z^{\max}$ is determined from kinematics by setting v_f to 10 m/s, and $\alpha = \sqrt{2k_BT/m}$. For our oven, at 400 ºC, $\acute{N}$ is approximately 4 x 10^{15} atoms/s. Using the Mathematica code found in Appendix A, for a slower with a radius of 1 cm we obtain the graph for R in Fig. 3.2.

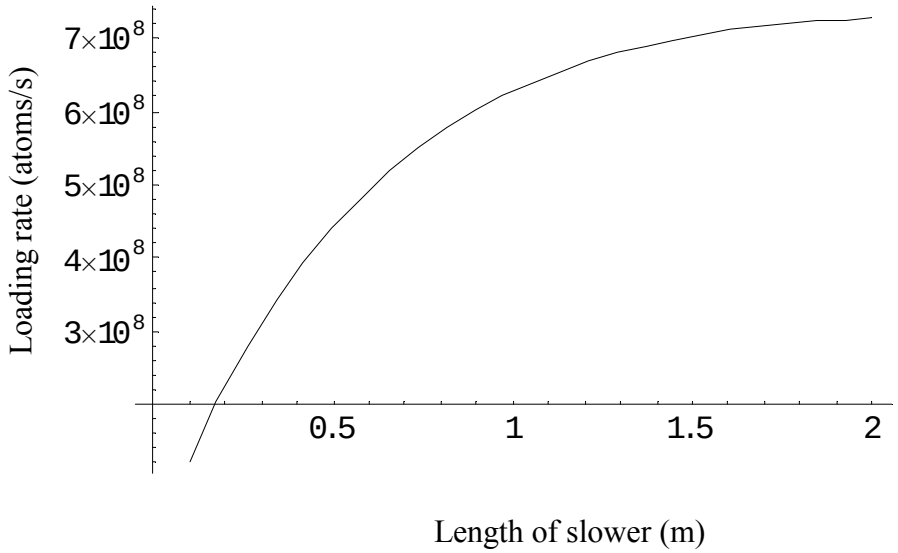

Figure 3.2. Trap loading rate R as a function of slower length.

From this graph, we see that when slower lengths fall below about one meter, the loading rate begins to drop steeply. In absolute terms, however, the decrease in loading rate is manageably small, amounting to much less than an order of magnitude even for very short slowers. Table 3.1 lists some representative values of R and l.

Length (m)	Rate (atoms/s)	Differs from 1-m-slower by factor of
1	6.28E+08	1
0.5	4.43E+08	0.7
0.4	3.82E+08	0.6
0.3	3.10E+08	0.5
0.2	2.24E+08	0.36
0.1	1.22E+08	0.19

Table 3.1. Trap loading rates at selected values of *l*.

A typical ^{6}Li MOT will saturate at densities on the order of 10^{11} atoms/cm^3, for a total of about half a billion atoms. Given loading times on the order of a few seconds (entirely reasonable for our system), these calculations indicate that even slowers much less than 0.5 m long will produce enough slow atoms for our purposes. Moreover, shorter slowers have several intrinsic advantages from a quasi-engineering perspective. I describe some of these advantages later in this section.

3.2 The Virtual Slower

Before we could select a final design for the new slower, we needed to know how several design parameters would affect its performance. To avoid the time and expense of constructing and testing physical prototypes, we used Mathematica software to construct a "virtual slower." This gave us considerable freedom to tinker with the slower design before we entered the actual construction and testing phase. In addition, we were able to check the accuracy of our simulation by creating a virtual slower with the same properties as our existing slower, and comparing its simulated performance with experimental results.

To create the Mathematica code for the virtual slower, we modified and added to a notebook written by Mike Gehm and Michael Stenner (Appendix A). In the original

notebook, a "coil" object has four parameters: radius, z-position, number of turns, and current. For example, Coil = {{.1, .05, 100, 1}} defines a coil with a 10-cm radius, position z = 5 cm, 100 turns, and 1 A current.

Defining coil objects in this fashion effectively packs all of a coil's turns into an infinitesimal volume. For many applications, the physical impossibility of doing this does not present any problems. However, since we wanted to know how wire size, coil "depth" (the number of layers of wire in the radial direction), and coil "width" (the number of winds in the z-direction per layer) affected the magnetic field, we needed a more physically realistic simulation.

Our new model uses an iterative method to create an idealized physical coil. Although it assumes perfect winding (impossible in practice, since for $N > 200$ the winding pattern becomes empirically chaotic), it does account for the increase in radius with each layer of wire (Δr) and for the increase in z-position with each individual wind (Δz), as in Fig. 3.3. This type of model coil is more complicated and more difficult to manipulate in Mathematica, but it is also a much better simulation of reality, so we expect its behavior to match that of a physical coil. A virtual slower is thus a collection of several such realistic coils, properly spaced and with the right dimensions.

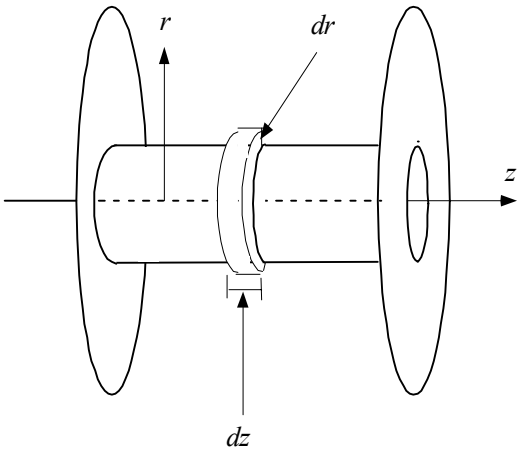

Figure 3.3. Coil geometry, with exaggerated *dr* and *dz*.

3.3 Current Requirements

Once we had a workable virtual slower, our next task was to determine how much current would have to pass through each coil to generate the correct total magnetic field. Knowing these currents was important not only for relatively minor design considerations (e.g. what type of wire to use) but also because current determines how much power – heat – the coils will produce, via the familiar $P = I^2 R$ relation. Thus, the magnitude of the currents will affect the design of the slower's cooling system.

To calculate the required currents, we used the modified Mathematica notebook to calculate the magnetic field each coil would produce at unit current (see Appendix A for the Mathematica code). The total magnetic field of the slower is thus the sum of these individual fields multiplied by variable currents I_i.

To find the numerical best-fit values of I_i, we employed Mathematica's nonlinear regression function to fit our "model" – the total magnetic field as a function of the I_i – to the "data" – the desired magnetic field we found in (2.10). The function's output is structured such that it returns the currents I_i that will yield the best magnetic field. Once we knew these best-fit currents, we plotted the slower's magnetic field and compared it to the ideal magnetic field. The sample comparison graph in Figure 3.4 demonstrates the close agreement between ideal and simulation.

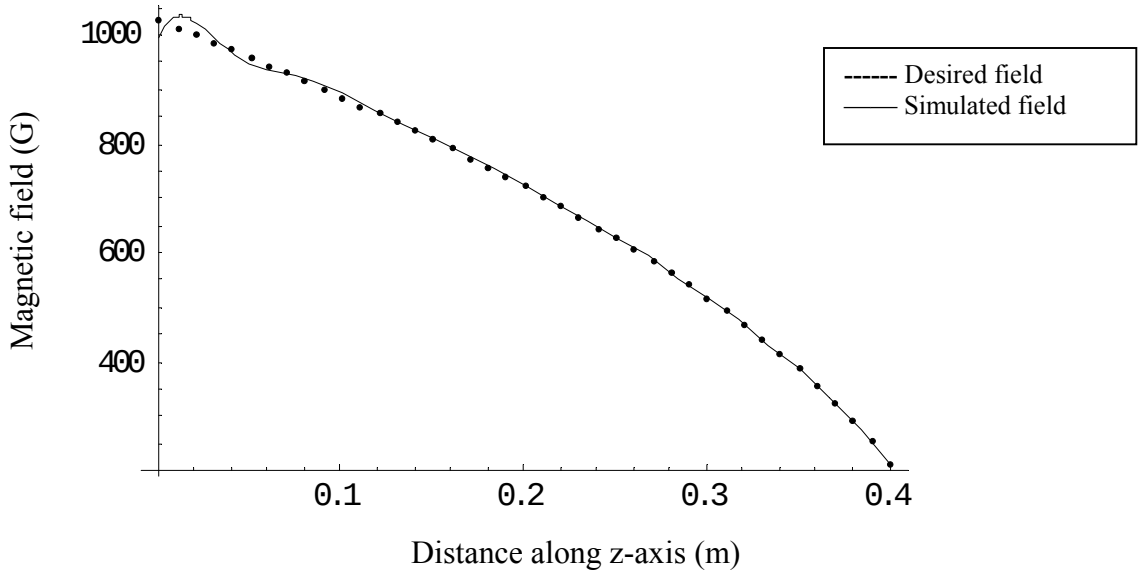

Figure 3.4. Sample plot of desired and simulated magnetic field.

3.4 Reconstructing the Existing Slower

To check the accuracy of our simulation, we created a virtual slower with the same characteristics as the existing slower. Table 3.2 contains a summary of the relevant

Parameter	Value
Δ	-200*10^6 Hz
α	0.62
final velocity	10 m/s
inner radius	0.0215 m
wire diameter	0.00268 m (12 AWG)
turns per coil	~390
coils	10

Table 3.2. Characterization of existing slower.

parameters. For some of these parameters, documentation on the original slower [2,3] contained conflicting information (as for initial velocity) or estimates (turns per coil, α). In such cases, we selected values towards the conservative end of the spectrum.

Our first model placed each simulated coil at evenly spaced intervals on the z-axis, from $z = 0$ to $z = 0.5$ m. This model produced best-fit currents within a few amps of the currents that run through the existing slower. However, it also gave rise to a "bumpy" magnetic field (Fig. 3.5) that did not fit the ideal taper very well (Fig. 3.6).

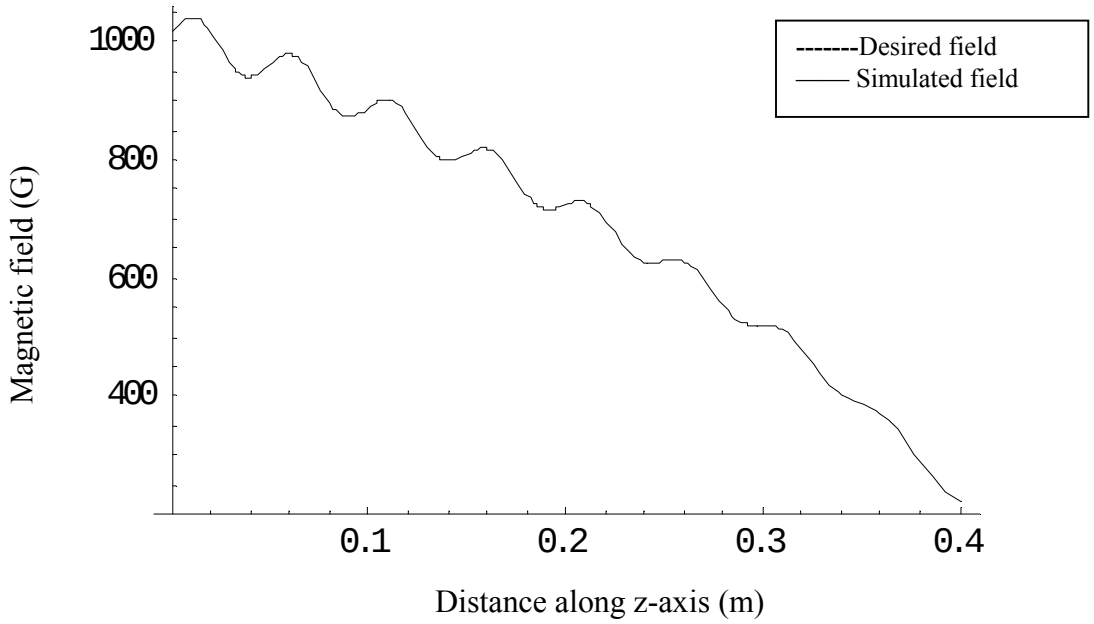

Figure 3.5. Plot of magnetic field generated by simulated 10-coil slower with evenly spaced coils, initial radius 2.1 cm, $N = 400$ turns.

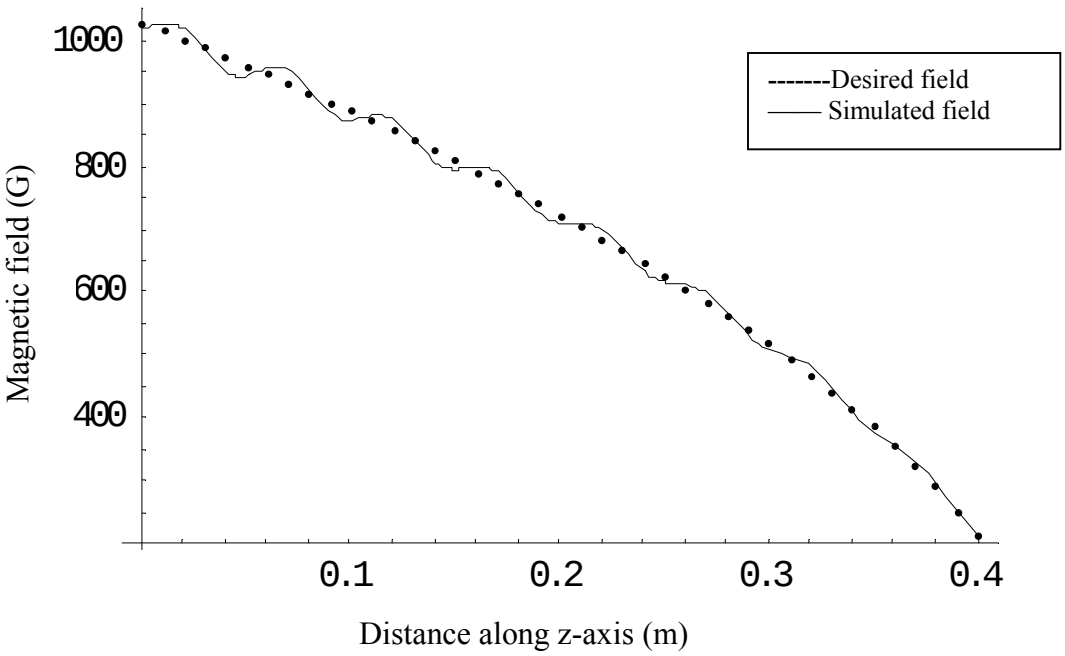

Figure 3.6. Plot of desired and simulated magnetic field for 10-coil slower with evenly spaced coils, initial radius 2.1 cm, $N = 400$ turns.

After re-checking our modeling process, we determined that the bumps were a consequence of the coil spacing. More precisely, our modeling method had placed each coil in the center of an evenly spaced slot wider than the coil itself. This means each coil is flanked on either side in the *z*-direction by small "gaps" that are free of wire and, consequently, do not generate any magnetic field. The bumps represent the center of a coil.

In our second model, we eliminated the bump problem by setting the start point of each new coil not in the center of an evenly spaced slot, but immediately after the previous coil ended. This new model also more accurately simulates the actual slower, in which wire fills up the space between copper discs that separate each coil from its neighbors, with no gaps except for small (0.050 inch) spaces between coils for the copper discs themselves. The model that produced Fig. 3.7 accounts for the discs, and as the

graph shows, the bumps do not appear. Near $z = 0.46$ m, the fit appears less accurate because the current in the simulated 10^{th} coil, as for the real 10^{th} coil, is set at –1.8 A rather than at the ideal value given by the fitting function. This detuning is necessary to keep the slowed atoms from drifting back into the slower [2].

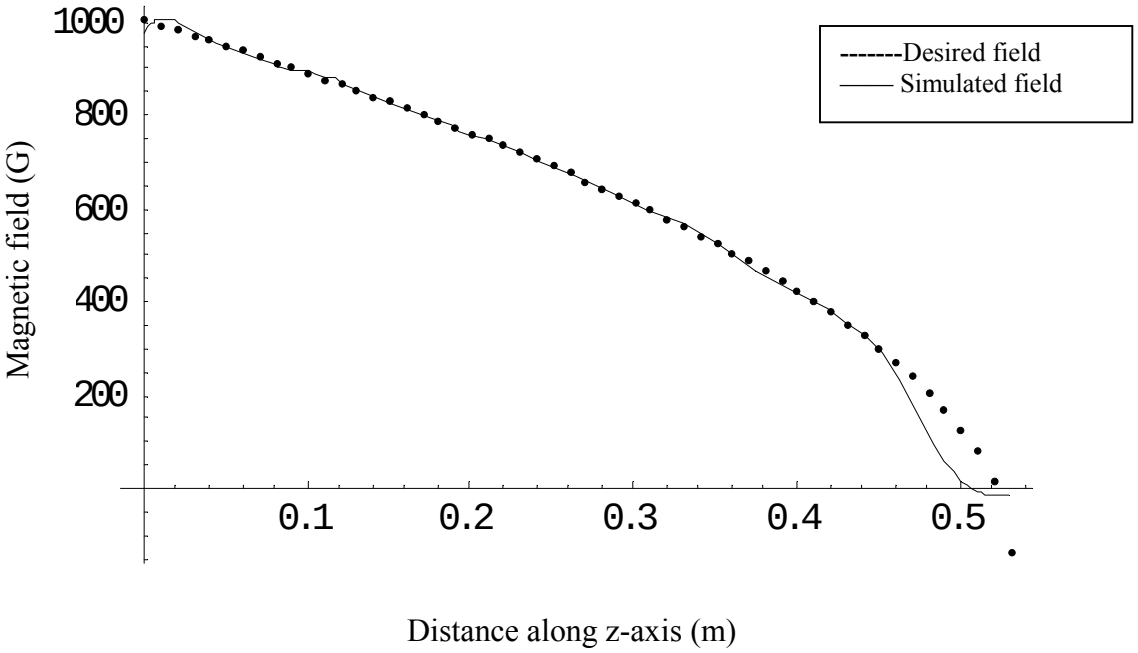

Figure 3.7. Plot of desired and simulated magnetic field for 10-coil slower with coils set next to each other, and all other paramaters unchanged from Figures 3.5 and 3.6.

In general, the currents our fitting function returned for each coil in the virtual slower matched the equivalent measured currents in the existing slower. Table 3.3 lists the experimental [2] and simulated optimum currents and two measures of the difference between them. Both the percent error and the absolute error indicate good agreement between model and experiment for the first (i.e. highest-current) coils. The quality of the agreement decreases for the later coils, but this is relatively unimportant because lower-current coils will contribute comparatively little to the overall heating and power

requirements of the system. Therefore, being able to predict their behavior to a high degree of accuracy is not absolutely necessary. Also, for all but one coil, our model recommended best-fit currents *higher* than the experimental values, which suggests that if our model errs, it does so on the conservative side. All of these factors led us to conclude that our model was performing well enough that we could now make changes to the existing design and be confident that the simulated results of the changes would agree with experimental reality.

coil	simulated current (A)	experimental current (A)	% error	absolute error (A)
1	14.76	13.73	7.50	1.03
2	10.17	10.48	-2.96	-0.31
3	9.8	9.51	3.05	0.29
4	8.76	8.49	3.18	0.27
5	8.01	7.53	6.37	0.48
6	7.01	6.79	3.24	0.22
7	6.19	5.33	16.14	0.86
8	4.6	4.12	11.65	0.48
9	4.42	2.9	52.41	1.52
10	-1.8	-1.8	0.00	0

Table 3.3. Comparing simulated and experimental currents.

3.5 Design Modifications

Our length calculations indicated that a shorter slower could still produce enough slow atoms for the MOT in a reasonable loading time (see section 3.1). Tests on the existing slower also showed that we could decrease the diameter of the slower's central pipe from $1\ ^{3}/_{8}$ inches (radius ~ 2.06 cm) to 1 inch (radius ~ 1.2 cm) without harming the ultra-high vacuum, and since the diameter of the laser beam is on the order of 1 cm, we will not lose

any of the cooling power at the lower diameter. The principle question, then, was what effect these two changes would have on the slower's required currents and the quality of the magnetic field curve fit.

For our first trial, we changed the initial radius to 1.2 cm and the length to 40 cm, and left all other parameters – number of coils, acceleration factor α, initial velocity, wire diameter, number of turns – unchanged. As the graph in Figure 3.8 shows, this configuration produces magnetic fields in good agreement with the ideal taper. And, as expected, the required currents decrease (Table 3.4).

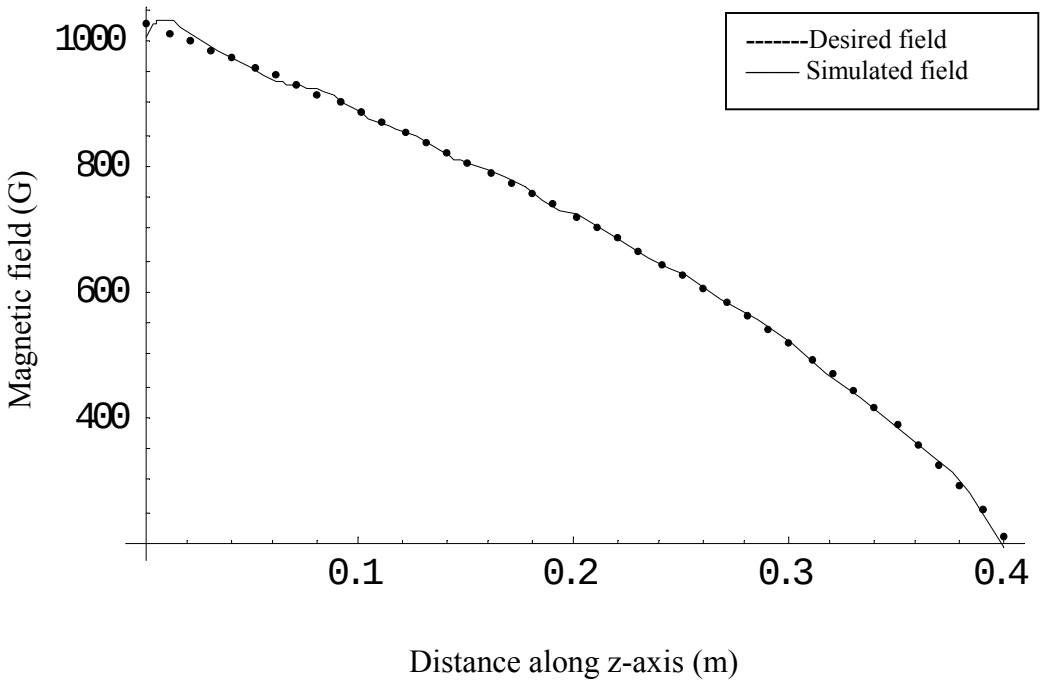

Figure 3.8. Plot of desired and simulated magnetic field for 40-cm slower with inner radius 1.2 cm. Other parameters unchanged from previous plots.

coil	current, simulated existing slower	current, 40-cm slower
1	14.76	13.71
2	10.17	8.94
3	9.8	8.64
4	8.76	7.8
5	8.01	7.2
6	7.01	6.5
7	6.19	5.75
8	4.6	5
9	4.42	3.92
10	-1.8	-1.8

Table 3.4. Comparing currents in existing slower and in 40-cm slower.

These data indicate that a slower with this design would perform as well as the existing slower. And, since $P = I^2 R$ is the Joule heating of the wire, the lower currents would translate into somewhat lower coil temperatures. Overall, though, this new design does not represent a major improvement on the original. In particular, the decrease in Joule heating is not enough to allow us to remove the slower magnets' water-cooling apparatus.

Our next model lowered the slower length further, to 30 cm, and correspondingly reduced the number of coils from 10 to 8. Thanks to a fortunate error in an earlier simulation, we knew that decreasing wire diameter would significantly reduce the current required[1], so we also used (simulated) 14 AWG solid copper wire instead of the original 12 AWG. Figure 3.9 shows that this configuration also gives excellent agreement between simulated and ideal magnetic fields. The quality of the fit for the 30-cm slower has dropped very little, if at all, from the original or 40-cm slowers.

[1] The reason for this change is intuitively simple. With smaller wire, one can pack more loops at lower radii, thus increasing the total current inside the pipe without increasing *N*, the number of turns. In classic experimentalist fashion, we did not predict this result, but once we saw it, we knew how to explain it and what to do with it.

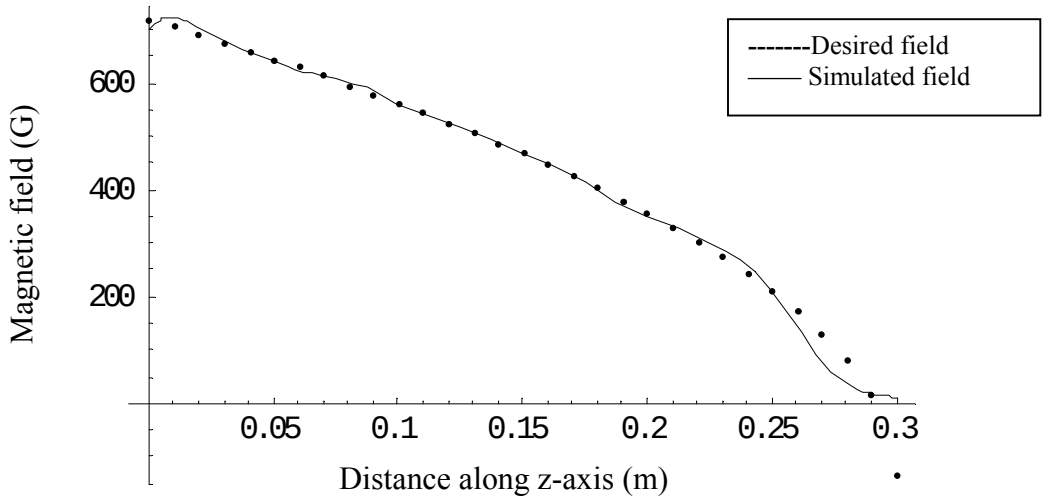

Figure 3.9. Plot of desired and simulated magnetic field for 30-cm slower.

coil	current, simulated existing slower	current, 30-cm slower
1	14.76	7.97
2	10.17	5.35
3	9.8	5.04
4	8.76	4.29
5	8.01	3.78
6	7.01	2.76
7	6.19	2.66
8	4.6	-0.58

Table 3.5. Currents in existing slower and 30-cm slower.

The differences in current required, by contrast, are striking. The data in Table 3.5 show marked decreases for all coils, including a reduction of nearly 50% for the highest-current coil.

Before we could determine how much power the highest-current coil would produce, we needed to know the coil's total resistance. The total length of wire L is

$$L = 2 \pi N_z \Sigma_{n=0\ldots21} (r_0 + n\, d) \qquad (3.6)$$

where N_z is the number of winds in the z-direction for each layer, r_0 is the coil's initial radius (i.e. the radius of the central pipe), and d is the diameter of the wire. The diameter

of 14 AWG wire is 2.32 mm, and for our system, $N_z = 19$ and $r_0 = 1.25$ cm. Performing the summation, we find L = 96.8 m. Since solid copper wire at 14 AWG has a resistivity per foot of 0.002525 Ω [6], the theoretical total resistance per coil is 0.8 Ω.

Given these values, a current of 7.97 A will generate Joule heating in the amount $P = I^2 R = 50$ watts. This is fairly low. By comparison, household light bulbs (which admittedly get rather warm) generally produce between 40 and 60 watts.

4 Coil Prototype

The results of the previous section demonstrated that the magnetic coils of a 30-cm slower could produce fields large enough to fit the ideal taper. They also indicated that the required currents would be low enough that a complicated water-cooling system would not be necessary. To test these results, we constructed a prototype of a single coil and measured the fields and temperatures it produced at various currents.

4.1 Construction

The raw materials for the prototype were 14 AWG solid copper wire, 0.005 inch thick copper sheeting and a 1-inch (outer) diameter brass pipe about 6 inches long. We cut the copper sheeting into two 6-inch diameter disks and bored 1-inch diameter holes at the center of each. This allowed us to slide the disks onto the brass pipe, leaving approximately 1.5 inches between disks for the coil of magnet wire. Although we had allowed essentially zero clearance and the press-fit was extremely tight, we also soft-soldered the joints between the disks and the pipe to ensure there would be no slippage during the wire winding process.

I used a lathe set on the slowest possible speed to wind the wire, stopping every few seconds to adjust the coils. Up to about N = 200 winds, the wire stacked up in a uniform

manner, but beyond that point the winding pattern became empirically chaotic. Due to a shortage of copper wire, I was only able to produce about 320 turns instead of the desired 400, but in other respects the coil was identical to those we had modeled. At this value of N, the diameter d_{filled} of the coil was approximately 3.75 inches, and Eq. 3.6 gives an estimated length about 230 feet, corresponding to a theoretical resistance of 0.57 Ω.

4.2 Testing

Once the winding process was complete, I connected the two ends of the coil to a power supply. The measured resistance of the entire coil was about 0.5 Ω. Based on this resistance and a current of 8 A, we expected to observe Joule heating on the order of 30 W.

I measured the temperature of the coil by attaching a thermocouple to the inside of the center brass pipe. At currents of 1-3 A – corresponding to the MOT end of the slower – the temperature difference between the coil and the surrounding air was negligible. At 8.5 A, the thermocouple gave a temperature reading of 60 ºC. At 10 A, the temperature approached 80 ºC. Beyond this point, I made no other temperature readings, both because we do not expect even the highest-current coil to require more than 8 A, and because the electrical tape holding the thermocouple in place was beginning to melt.

All measurements were taken in the absence of any special air-cooling mechanism. We have observed in the previous slower that adding a whisper fan reduces the maximum temperature by 15-20 ºC. Since we do not need the slower to run cool enough for us to be able to touch it while it is running, only cool enough that the solder and the copper

wire do not melt, these tests show that a slower with the new design will not need a complicated water cooling system.

Once we were certain the coil was in no danger of melting at any reasonable current, we used a Hall probe to measure the magnetic field it produced. Figure 4.1 shows the magnetic field of the prototype coil at 8 A. At this current, the maximum field was 570 G. Increasing the current to 9 A raised this maximum to 650 G, and at 10 A, the peak magnetic field was 710 G.

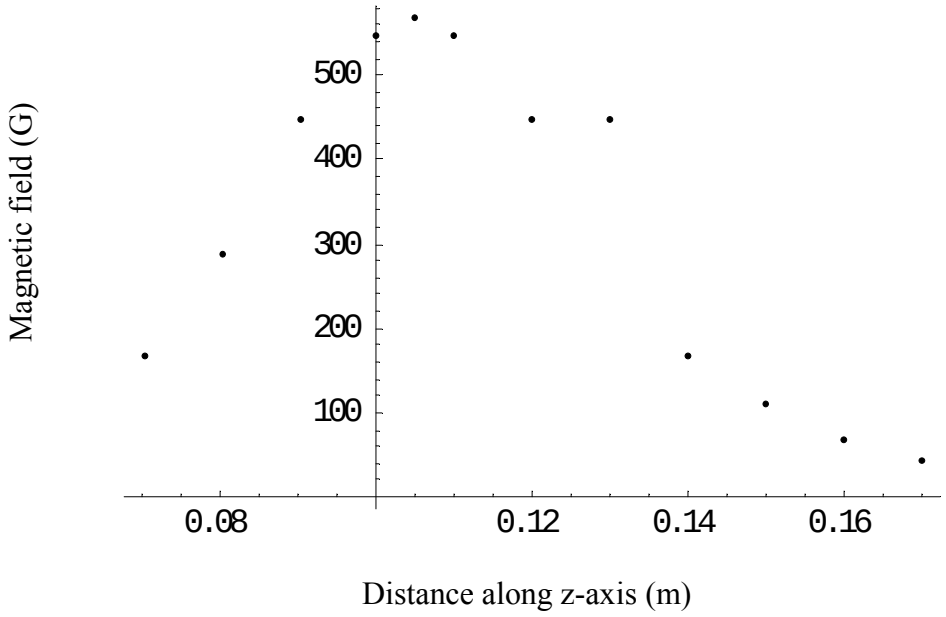

Figure 4.1. Magnetic field of prototype coil at 8 A.

To check the accuracy of our model, I used the Mathematica magnetic field code to simulate a slower with N=323 turns (roughly equal to the prototype) in each coil. At this value of N, the fitting function returned a current of 9.35 A for the first coil. According to the program, a single coil at this current should generate a peak magnetic field of 570 G. Note that although the maximum required field for the entire 8-coil system is 700 G, the superposition of the fields means that individual coil outputs can be much lower.

In the prototype coil, a current of 9.35 A generated a maximum field of 670 G. This means the prototype actually performed slightly *better* than the model's prediction. Figure 4.2 contains a plot of the simulated and actual magnetic fields at 8 A.

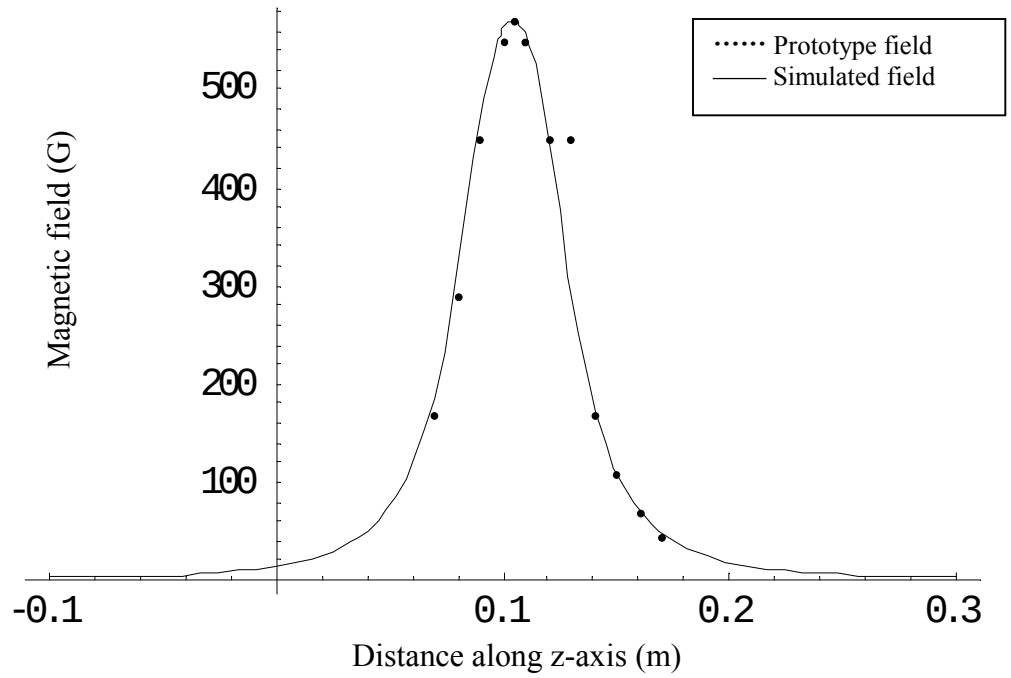

Figure 4.2. Magnetic fields of simulated and actual prototype coil.

After we finished testing, we unwound the wire from the coil and found it measured 240 feet. A perfectly wound coil would have required about 10 feet less wire (see Eq. 3.6). This extra length confirms our imperfect winding.

5 Construction

Based on the tests of the prototype, we concluded that our new design was viable, and would require only minor modifications. In this section I describe these modifications and the construction of the full 8-coil slower.

5.1 Modifications and Final Design

The prototype's 320 turns of wire filled just over half the diameter of the copper disks, so in the final design we reduced the disks' diameter to 5 inches. We could have reduced the diameter further without running out of room for the wire, but we chose to make only a conservative reduction because the extra copper makes a good heat sink. We also changed the material and inner diameter of the central pipe. The brass pipe we used before worked well in the prototype, but is poor material for an ultra high vacuum. The final design uses #304 stainless steel instead. The type of wire (14 AWG, coated solid copper) and method of fitting the disks to the pipe (press fit, soft solder) did not change.

In the prototype, we could leave the two ends of wire dangling when we attached them to the power supply, but the actual slower required a more permanent means of connection. We therefore included eight Delrin bars (Delrin is a readily available and easily machined plastic) in the final design to act as platforms for connecting the ends of each coil to its power supply terminals. Each bar fits into the space between two copper

disks, and contains four threaded holes: two ¼-20 on the top for connections, and one $^{3}/_{8}$ -16 on each side for screws that slide into narrow slits in the disks and hold the bar in place. Besides serving as a connection mount, these bars will also keep the wire from unwinding.

Appendix B contains the shop drawings for the copper disks, Delrin bars, and assembled slower drawn with the TurboCAD program.

5.2 Assembly and Recommendations

Once the main body of the slower was built, I followed the same procedures I employed in the prototype to wind the wire, with one difference: for each coil, I counted 400 turns and then added about a dozen extra to compensate for possible undercounting. I estimate each coil contains between 400 and 420 turns.

Attaching the ends of each coil to the Delrin bars proved more difficult than expected because the top holes were set very close together. In order to attach both ends without letting them touch at any point, it was necessary to use one tall and one short screw. Although this adjustment was hardly "mission-critical," it was definitely inconvenient, and any future Zeeman slower designers should use a wider spacing for the connections.

Because stainless steel does not take solder particularly well, the machinists in the Physics Shop had some difficulties getting the copper disks to stay in place. During the winding process, the end disk became partially detached at the solder joint, and had to be secured with a hose clamp. Again, the problem is not mission-critical, but in future slowers, high-temperature silver solder would be a better choice.

6 Future Directions

Although all the tests and modeling we have done so far indicate the new design is likely to succeed, the new Zeeman slower must still pass two distinct stages of testing before we can draw our final conclusions. In this section I give a brief overview of these two stages.

6.1 Magnetic Field Tests

Our first step will be to use the Hall probe to measure the field of each coil individually, similar to what we did for the prototype, and compare these measurements with the Mathematica simulation. If any of the coils is not working properly, it should be fairly easy to fix; one of the advantages of using a slower with eight independent coils is that unlike Christmas lights, if one goes out, they do not all go out. Thus, even if "fix" means "take all the wire off one coil and wind new wire in its place because there may be an electrical short somewhere," the other coils and the supporting structure should emerge unscathed.

Once we have determined that each coil is working properly, we will measure the entire slower's magnetic field with the Hall probe and compare it with the Mathematica

simulation. We will also measure the temperature response of each coil at the desired current.

6.2 Implementing the Slower

After the slower passes the preliminary magnetic field tests, we will need to clean the inside of the steel pipe thoroughly and weld flanges onto either end before we can attach it to the vacuum system. The final test will be to show that the new design can produce slow lithium atoms and transfer them into the MOT at high trap loading rates. We can carry out this test with the existing oven and dye laser; however, we expect the new slower to become part of an entirely separate cold-atoms experiment, along with a new oven and laser.

7 Conclusions

The results of the extensive, rigorous modeling process described in this document indicate that the slower we constructed has a very high probability of success. Our model takes into account all the relevant physical properties of the slower, and the tests we conducted on the prototype demonstrate that it does an excellent job of predicting the actual length of wire required and the total resistance of the coil. Most importantly, the modeled magnetic field matches the field generated by the prototype almost exactly, with no bizarre effects or anomalies to worry about.

Our model also shows that a shorter slower can meet design criteria, at least in theory. If the new Zeeman slower passes the tests outlined in the previous section – and our thorough modeling indicates that there is no reason why it should not – the new design will represent a significant improvement and simplification in slower technology, outpacing both the existing slower in JETLab and slowers used in other groups (e.g. Ketterle, MIT) which require specialized coils and cooling systems to function. We have shown that the process of constructing the slower was fairly straightforward, and we predict that maintaining it will present few additional problems; besides its compact size, the new slower uses currents low enough that it will not need any water cooling, and should therefore prove both durable and very easy to run.

This document contains information on all the work we did to design and build the new Zeeman slower, and is intended to serve as a manual for future designers.

Appendix A: Mathematica Code

I. Length

Setting up length equations:

```
vzmax[l_] := Sqrt[vf^2 + 2*a*l]
vrmax[l_] :=
 r0/((vzmax[l] - vf)/a + df/vf + di/vzmax[l])
vrmax[.3]
```

0.634352

```
r[l_] := 4*10^15*(1 - Exp[(-vzmax[l]^2)/alpha^2])
  (1 - Exp[(-vrmax[l]^2)/alpha^2])
```

Setting parameters:

```
alpha = 1363
```

1363

```
r0 = .01
```

0.01

```
vf = 10
```

10

```
a = .75 * 1.83*10^6
```

1.3725×10^{6}

```
df = .15
```

0.15

```
di = .10
```

0.1

Graphing r[l], the trap loading rate:

```
Plot[4*10^15*r[l], {l, .1, 2}]
```

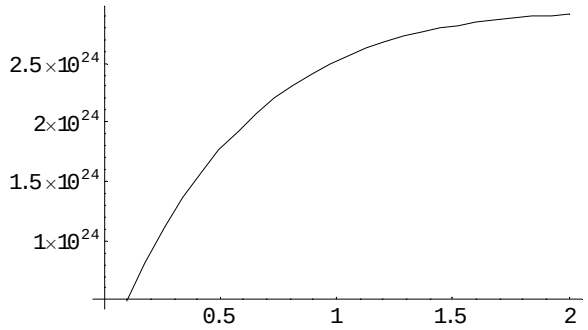

- Graphics -

Calculating R for sample lengths l:

```
r[.1]
```
1.22112×10^8
```
r[.2]
```
2.24452×10^8
```
r[.5]
```
4.43091×10^8
```
r[.05]
```
6.36009×10^7
```
r[.3]
```
3.10268×10^8
```
r[.4]
```
3.82403×10^8

II. Magnetic Field Modeling

Code in existing Mathematica notebook:

Definitions

Constants

```
μ0 = 4 Pi * 10^-3; (* Gives answers in Gauss *)
```

Calculation Functions

These functions calculate the radial and axial field for a single coil.

```
Bz[r_, z_, coil_] :=
 coil[[3]] * coil[[4]] * (μ0 / (2 Pi)) / Sqrt[(coil[[1]] + r)^2 + (z - coil[[2]])^2] *
  (EllipticK[4 coil[[1]] r / ((coil[[1]] + r)^2 + (z - coil[[2]])^2)] +
    ((coil[[1]]^2 - r^2 - (z - coil[[2]])^2) / ((coil[[1]] - r)^2 + (z - coil[[2]])^2)) *
     EllipticE[4 coil[[1]] r / ((coil[[1]] + r)^2 + (z - coil[[2]])^2)])
Br[r_, z_, coil_] := coil[[3]] * coil[[4]] * z^2 *
  (μ0 / (2 Pi r)) / Sqrt[(coil[[1]] + r)^2 + (z - coil[[2]])^2] *
  (-EllipticK[4 coil[[1]] r / ((coil[[1]] + r)^2 + (z - coil[[2]])^2)] +
    ((coil[[1]]^2 + r^2 + (z - coil[[2]])^2) / ((coil[[1]] - r)^2 + (z - coil[[2]])^2)) *
     EllipticE[4 coil[[1]] r / ((coil[[1]] + r)^2 + (z - coil[[2]])^2)])
```

These functions calculate the field for all of the coils listed in "coils".

```
AxialField[r_, z_, coils_] :=
 Module[{}, TempFunc[coil_] := Bz[r, z, coil];
  Plus @@ Map[TempFunc, coils, {1}]]
RadialField[r_, z_, coils_] :=
 Module[{}, TempFunc[coil_] := Br[r, z, coil];
  Plus @@ Map[TempFunc, coils, {1}]]
```

This function calculates the field magnitude at any point using the previous functions.

```
FieldMag[r_, z_, coils_] :=
 If[r == 0, AxialField[r, z, coils],
  Sqrt[AxialField[r, z, coils]^2 + RadialField[r, z, coils]^2]]
```

Tools for generating "coils" list

```
WithTurns[precoil_, turns_] :=
 Module[{}, TempFunc[coil_] := Append[coil, turns];
  Map[TempFunc, precoil, {1}]]
WithCurrent[precoil_, current_] :=
 Module[{}, TempFunc[coil_] := Append[coil, current];
  Map[TempFunc, precoil, {1}]]
WithTurnsAndCurrent[precoil_, turns_, current_] :=
 WithCurrent[WithTurns[precoil, turns], current]
```

Description

What this notebook does

This notebook calculates the magnetic field at any point in space for an arbitrary number of coils. Each coil can have a different position, size, number of turns, and current. The one restriction is that all coils must share the same axis.

How to use this notebook

First, you must make your "coils" list. This is a list of lists. You have one internal list for each coil. Each of these internal coil (singular) lists contains the radius of the coil (in meters), the position of the coil (in meters), the number of turns, and the current (in Amperes). The following coils list defines one coil with a radius of 10 cm, position of z = 5 cm, 100 turns, and a 1 mA current.

```
ExampleCoils = {{.1, .05, 100, .001}};
```

Once this is defined, you can determine the axial field (parallel to z), radial field (perpendicular to z), and field magnitude at any point (r, z) with the functions: AxialField, RadialField, and FieldMag. each of these functions takes r, z, and your coils list. All of these functions return the magnetic field in Gauss. Example:

```
Plot[AxialField[0, z, ExampleCoils], {z, -.1, .1}];
```

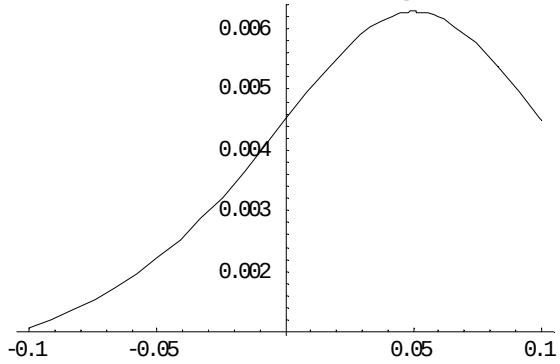

Generating coils lists

There are several functions to help you generate coils lists.

The function "Helmholtz" takes the parameters for a coil list (r, z, turns, current) and returns a coils list with two identical coils. One has the parameters you specified, and the other has a position of -z.

The function "TrueHelmholtz" takes the same parameters except that it does not take a radius. The radius is automatically set to 2z.

The functions "AntiHelmholtz" and "TrueAntiHelmholtz" work identically except that the mirror coil has the opposite current.

```
ExampleCoils = AntiHelmholtz[.4, .15, 100, .001];
Plot[AxialField[0, z, ExampleCoils], {z, -.1, .1}];
```

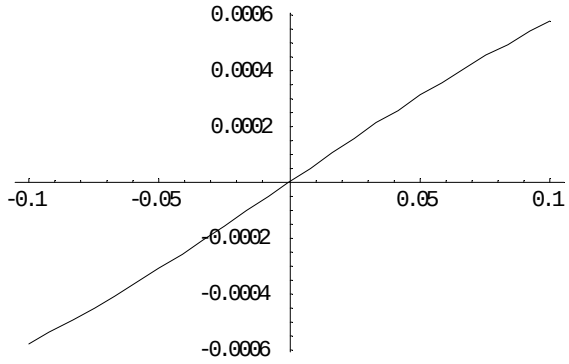

There are also functions for helping generate a list of several coils with the same current or number of turns. To use these functions, create a "precoils" list without the current or without both current and turns.

```
ExamplePreCoils = {{.1, -.1}, {.1, .1}}
{{0.1, -0.1}, {0.1, 0.1}}
NewExamplePreCoils = WithTurns [ExamplePreCoils , 30]
{{0.1, -0.1, 30}, {0.1, 0.1, 30}}
ExampleCoils = WithCurrent [NewExamplePreCoils , .4]
{{0.1, -0.1, 30, 0.4}, {0.1, 0.1, 30, 0.4}}
```

Or simply

```
ExampleCoils = WithTurnsAndCurrent [ExamplePreCoils , 30, .4]
{{0.1, -0.1, 30, 0.4}, {0.1, 0.1, 30, 0.4}}
```

Function Summary

coils =
coils = Helmholtz[rad, z, turns, I]
coils = TrueHelmholtz[z, turns, I]
coils = AntiHelmholtz[rad, z, turns, I]
coils = TrueAntiHelmholtz[z, turns, I]
coils = WithCurrent[precoils, I] (where precoils is a coils list with the current missing)
precoils = WithTurns[preprecoils, turns] (where preprecoils is a coils list with both currents and turns missing)

AxialField[r, z, coils]
RadialField[r, z, coils]
FieldMag[r, z, coils]

Example

List of coils. Each coil is a list of (coil radius, coil z position, number of turns, and current). Distances are in meters, and current in Amperes.

```
coils = Helmholtz [12.25 * .0254 , 6.125 * .0254 , 30, 1];
RadiusOfInterest  = .1;
Plot [AxialField [0, z, coils ],
  {z, -RadiusOfInterest  , RadiusOfInterest  }, PlotRange → All];
Plot [AxialField [r, 0, coils ], {r, -RadiusOfInterest  , RadiusOfInterest  },
  PlotRange → All];
```

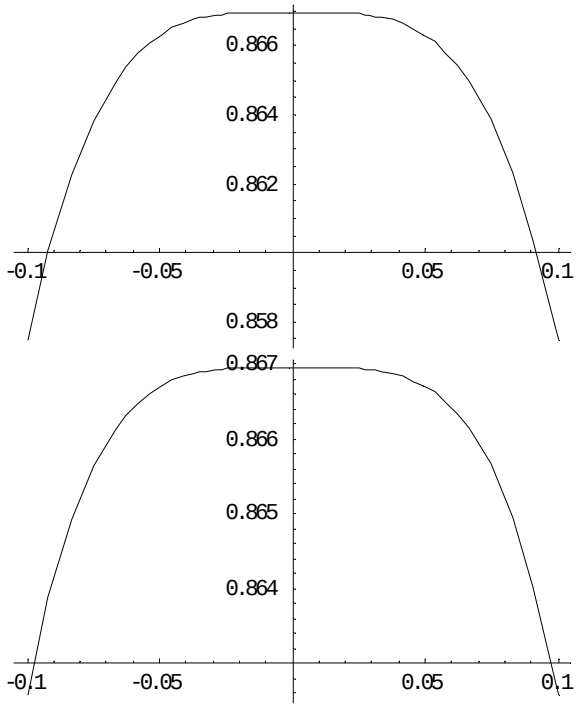

Modifications to Existing Notebook:

Setting up the iterated coils:

```
RegularSpacedRealCoil[InitR_, RStep_, RNum_, InitZ_, ZStep_, ZNum_, Current_] :=
 Flatten[Table[{InitR + i * RStep, InitZ + j * ZStep, 1, Current}, {i, 0, RNum - 1},
   {j, 0, ZNum - 1}], 1]
```

Defining constants and expressions for velocity and B-field:

```
h = 6.626*10^-34;
delta = -200*10^6;
lambda = 671.0*10^-9;
MB = 9.27*10^-28;
a = .6*1.83*10^6;
vf = 10;
l = .3

InitV[vf_, l_, a_] := Sqrt[vf^2 - l* 2*-a];
bz[z_] := (h / MB) * (delta + (1 / lambda) * Sqrt[InitV[vf, l, a]^2 - (2*a*z)])
Plot[bz[z], {z, 0, .3}]
data = Table[{z, bz[z]}, {z, 0, .3, .01}];
```

Use Nonlinear Fit package
Building the virtual slower, coil by coil:

```
<< Statistics`NonlinearFit`
SRad = 0.0125;
RInc = .002032;
RTurn = 17.0;
SZInc = .002032;
SZTurn = 19.0;
SingleCoil1 = RegularSpacedRealCoil[SRad, RInc, RTurn, -.019, SZInc, SZTurn, 1];
SingleCoil2 = RegularSpacedRealCoil[SRad, RInc, RTurn, .0211, SZInc, SZTurn, 1];
SingleCoil3 = RegularSpacedRealCoil[SRad, RInc, RTurn, .0612, SZInc, SZTurn, 1];
SingleCoil4 = RegularSpacedRealCoil[SRad, RInc, RTurn, .1013, SZInc, SZTurn, 1];
SingleCoil5 = RegularSpacedRealCoil[SRad, RInc, RTurn, .1414, SZInc, SZTurn, 1];
SingleCoil6 = RegularSpacedRealCoil[SRad, RInc, RTurn, .1815, SZInc, SZTurn, 1];
SingleCoil7 = RegularSpacedRealCoil[SRad, RInc, RTurn, .2216, SZInc, SZTurn, 1];
SingleCoil8 = RegularSpacedRealCoil[SRad, RInc, RTurn, .2617, SZInc, SZTurn, 1];
```

Test plot: what does a single coil's magnetic field look like?

```
Plot[AxialField[0, z, SingleCoil1], {z, 0, .1}]
```

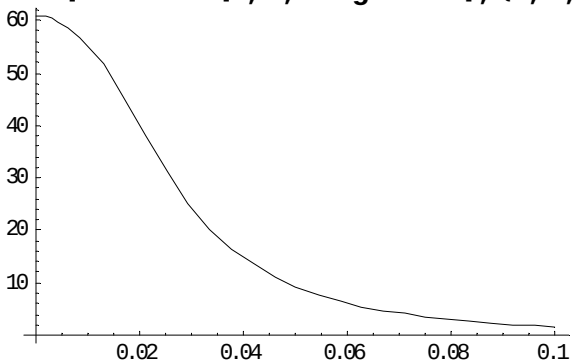

- Graphics -

Defining magnetic fields for each coil using the AxialField function:

```
B1[z_] := AxialField[0, z, SingleCoil1]
B2[z_] := AxialField[0, z, SingleCoil2]
B3[z_] := AxialField[0, z, SingleCoil3]
B4[z_] := AxialField[0, z, SingleCoil4]
B5[z_] := AxialField[0, z, SingleCoil5]
B6[z_] := AxialField[0, z, SingleCoil6]
B7[z_] := AxialField[0, z, SingleCoil7]
B8[z_] := AxialField[0, z, SingleCoil8]
Bfield[i1_, i2_, i3_, i4_, i5_, i6_, i7_, i8_] :=
 i1 * B1[z] + i2 * B2[z] + i3 * B3[z] + i4 * B4[z] + i5 * B5[z] + i6 * B6[z] +
  i7 * B7[z] + i8 * B8[z]
Clear[i1, i2, i3, i4, i5, i6, i7, i8]
```

Performing the nonlinear regression, output of values:

```
NonlinearRegress[data, Bfield[i1, i2, i3, i4, i5, i6, i7, i8], {z},
 {i1, i2, i3, i4, i5, i6, i7, i8}]
BestFitParameters → {i1 → 9.34725, i2 → 6.60703, i3 → 6.15811,
  i4 → 5.28855, i5 → 4.61755, i6 → 3.44819, i7 → 3.12214, i8 → -0.475744},
```

Using the best-fit currents to plot the simulated magnetic field:

```
p1 = Plot[9.35 * B1[z] + 6.61 * B2[z] + 6.16 * B3[z] + 5.29 * B4[z] + 4.62 * B5[z] +
   3.44 * B6[z] + 3.12 * B7[z] + -.48 * B8[z], {z, 0, .3}]
```

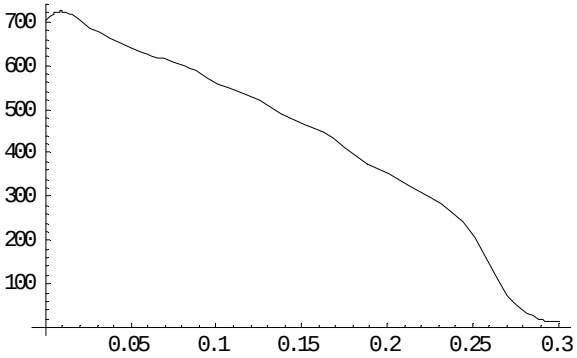


```
- Graphics -
```

Plot of the desired magnetic field taper:

```
p2 = ListPlot[data]
```

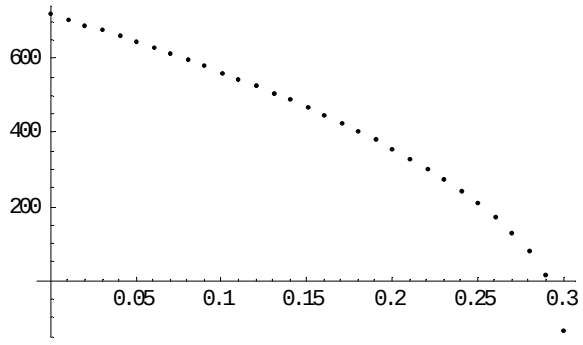

-Graphics-

Simulated (best-fit) magnetic field and ideal magnetic field:

```
Show[p1, p2]
```

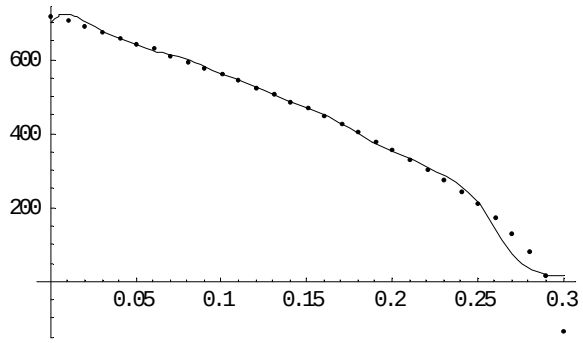

Plot of the maximum-current coil at 9.35 A (part of prototype-testing process):

```
p3 = Plot[9.35*B1[z], {z, -.1, .3}]
```

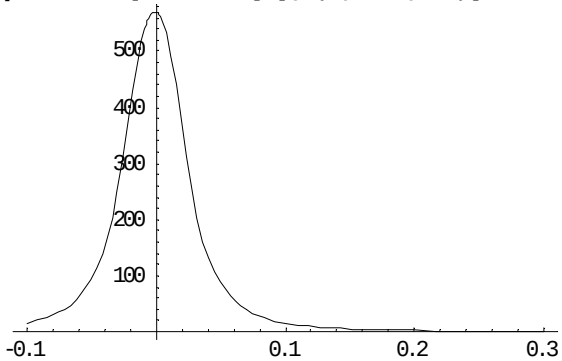

-Graphics-

Calculating the maximum magnetic field of this coil at 9.35 A:

```
9.35*B1[-0.001]
570.782
```

Comparing the prototype data with the simulation:

```
realdata = {{.17, 45}, {.16, 68}, {.15, 110}, {.14, 170}, {.13, 450},
  {.12, 450}, {.11, 550}, {.105, 570}, {.1, 550}, {.09, 450}, {.08, 290},
  {.07, 170}}
{{0.17, 45}, {0.16, 68}, {0.15, 110}, {0.14, 170}, {0.13, 450}, {0.12, 450},
 {0.11, 550}, {0.105, 570}, {0.1, 550}, {0.09, 450}, {0.08, 290}, {0.07, 170}}

p4 = ListPlot[realdata]
```

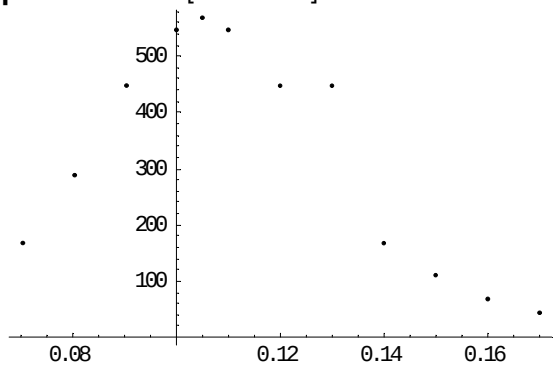


```
- Graphics -
```

Prototype data and simulation on same graph:

```
Show[p3, p4]
```

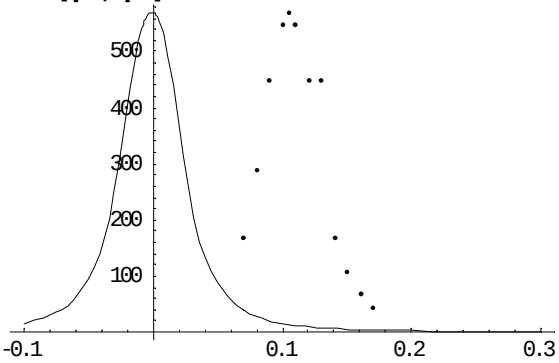


```
- Graphics -
```

Appendix B:
Shop Diagrams for Slower

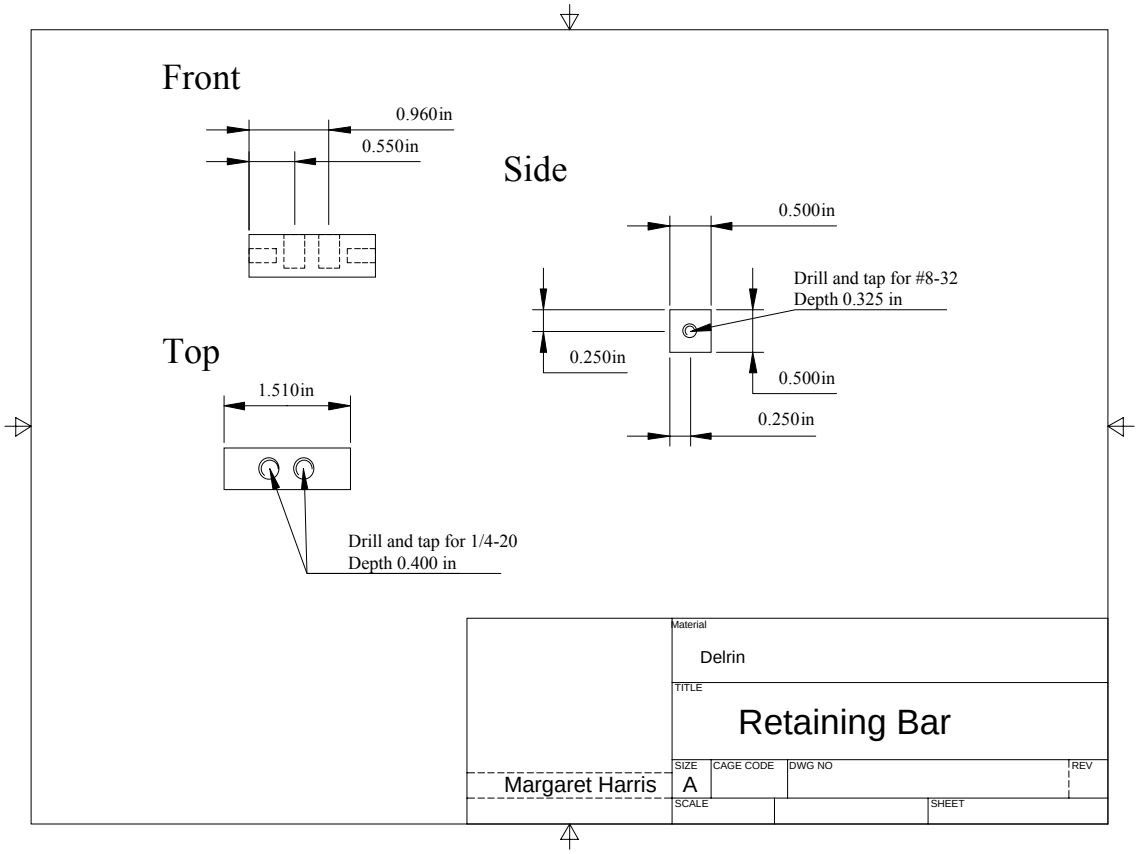

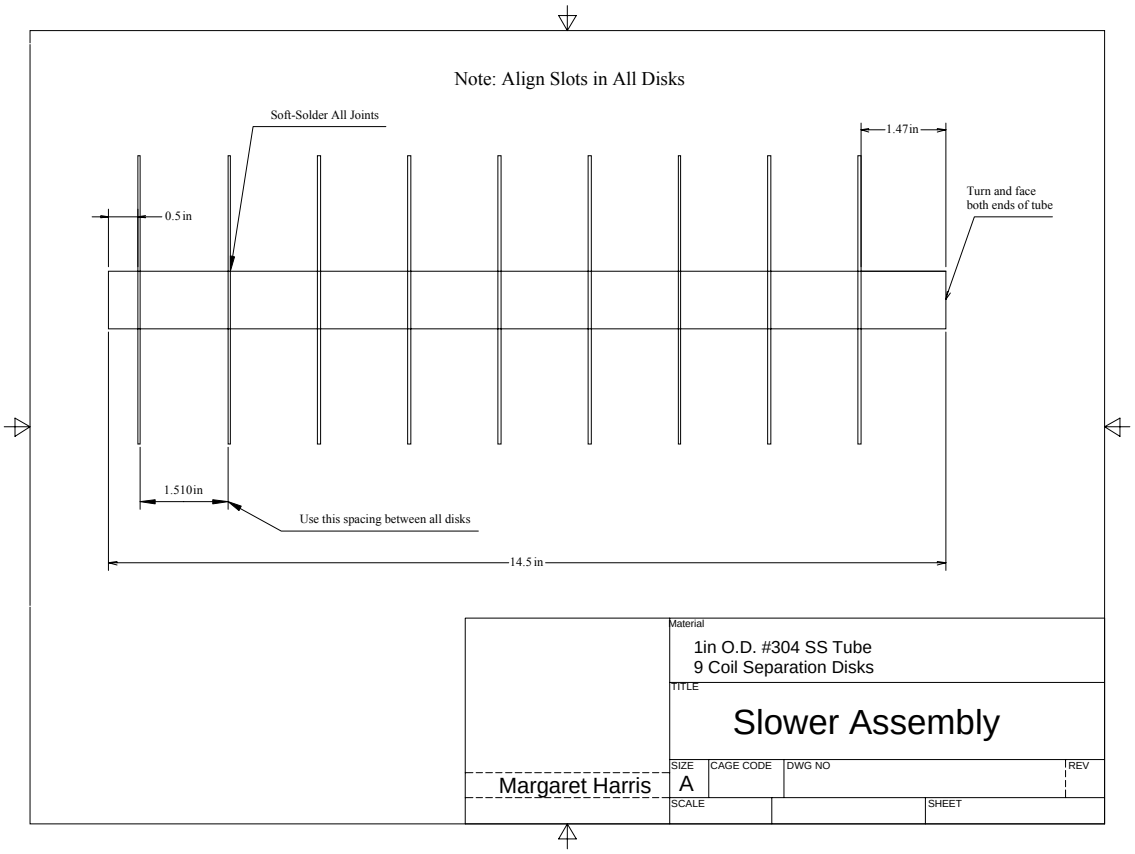
Note: Align Slots in All Disks
Soft-Solder All Joints
1.47in
Turn and face
both ends of tube
0.5 in
1.510in
Use this spacing between all disks
14.5 in
Material
1in O.D. #304 SS Tube
9 Coil Separation Disks
TITLE
Slower Assembly
Margaret Harris
SIZE
A
CAGE CODE
DWG NO
REV
SCALE
SHEET

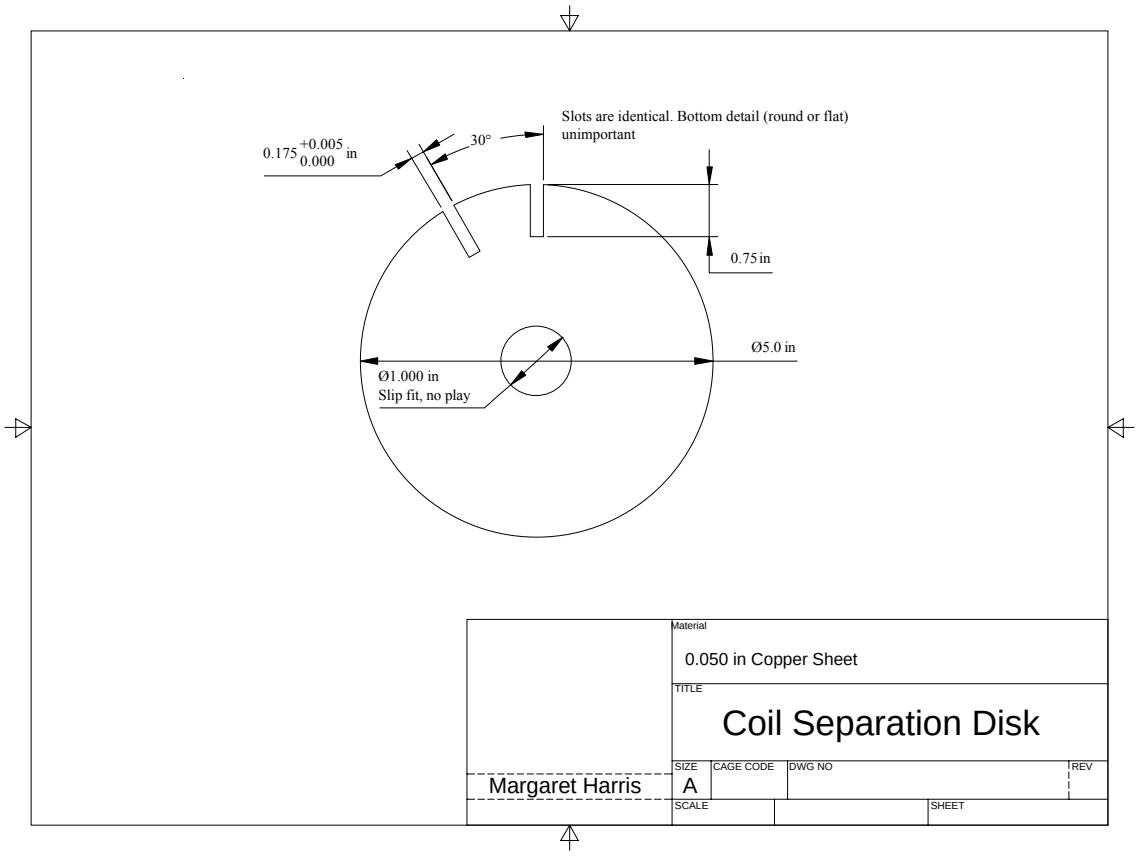
Slots are identical. Bottom detail (round or flat) unimportant
0.175 +0.005 0.000 in
30°
0.75 in
Ø5.0 in
Ø1.000 in
Slip fit, no play
Material
0.050 in Copper Sheet
TITLE
Coil Separation Disk
Margaret Harris
SIZE
A
CAGE CODE
DWG NO
REV
SCALE
SHEET

Bibliography

[1] C. Kittel and H. Kroemer. *Thermal Physics*. W. H. Freeman, New York, second edition, 2002.

[2] T. A. Savard. Raman Induced Resonance Imaging of Trapped Atoms. Ph.D Dissertation at Duke University, 1998.

[3] C.A. Baird. Design and Characterization of a Multi-Coil Zeeman Slower. Master's Thesis at Duke University, 1996.

[4] Georgia State Hyperphysics Website. "Zeeman Interaction." Available at http://hyperphysics.phy-astr.gsu.edu/hbase/quantum/zeeman.html.

[5] M. E. Gehm. Preparation of an Optically-Trapped Degenerate Fermi Gas of ^{6}Li: Finding the Route to Degeneracy. Ph.D. Dissertation at Duke University, 2003.

[6] T. L. Floyd. *Electric Circuit Fundamentals.* Merril, second edition, 1991.